A Computational Fluid Dynamics Approach to Nucleation in the Water−Sulfuric Acid System

E. Herrmann,*,† D. Brus,‡,§ A.-P. Hyvärinen,‡ F. Stratmann,∥,⊥ M. Wilck,⊥ H. Lihavainen,‡ and M. Kulmala†

Department of Physics, University of Helsinki, Finland, Finnish Meteorological Institute, Helsinki, Finland, Laboratory of Aerosol Chemistry and Physics, Institute of Chemical Process Fundamentals ASCR, Prague, Czech Republic, Leibniz-Institut für Troposphärenforschung, Leipzig, Germany, and Particle Dynamics GmbH, Leipzig, Germany

Received: April 19, 2010; Revised Manuscript Received: June 3, 2010

This study presents a computational fluid dynamics modeling approach to investigate the nucleation in the water−sulfuric acid system in a flow tube. On the basis of an existing experimental setup (Brus, D.; Hyvärinen, A.-P.; Viisanen, Y.; Kulmala, M.; Lihavainen, H. *Atmos. Chem. Phys.* **2010**, *10*, 2631−2641), we first establish the effect of convection on the flow profile. We then proceed to simulate nucleation for relative humidities of 10, 30, and 50% and for sulfuric acid concentration between 10^9 to 3×10^{10} cm^{-3}. We describe the nucleation zone in detail and determine how flow rate and relative humidity affect its characteristics. Experimental nucleation rates are compared to rates gained from classical binary and kinetic nucleation theory as well as cluster activation theory. For low *RH* values, kinetic theory yields the best agreement with experimental results while binary nucleation best reproduces the experimental nucleation behavior at 50% relative humidity. Particle growth is modeled for an example case at 50% relative humidity. The final simulated diameter is very close to the experimental result.

1. Introduction

Besides health effects and their impact on visibility, aerosol particles in the atmosphere affect the radiative balance and thus the global temperature directly,[2] indirectly,[3] and semidirectly.[4] The formation of new particles in the atmosphere has received much attention over the last years, and particle formation events have been observed almost everywhere on earth.[5] Considerable efforts have been made to understand the mechanisms underlying these events, be it field, or laboratory measurements, or computer simulations on nucleation and the aerosol dynamics processes involved. However, the process of new particle formation is not yet fully understood.

Sulfuric acid has been identified to likely play a key role in atmospheric nucleation.[6] The binary nucleation of water and sulfuric acid may explain particle formation in the stratosphere or the upper troposphere.[7] However, various theoretical approaches require additional substances to explain the observed nucleation events in the lower troposphere. Ternary nucleation also involving ammonia[8] has long been a favorite, while newer suggestions include, for example, organics.[9,10] Finally, new experiments at ambient sulfuric acid concentrations have produced similar nucleation rates as observed in the atmosphere—without a third species present.[11] Recent geo-engineering approaches[12,13] rely on the central role of sulfuric acid and suggest ways to increase the H_2SO_4 contents of the atmosphere to stimulate aerosol production and thus cool the atmosphere.

Reiss et al. were among the first to perform laboratory experiments on the binary nucleation of sulfuric acid and water.[14] Over the years, the process was studied by various groups using various techniques; however, the more recent experiments[11,15−18] all rely on a flow-based measurement technique. It has to be pointed out that these laboratory measurements were typically conducted at temperatures 10−30 K above those observed during atmospheric nucleation events.

In order to characterize the flow and to better understand the experimental conditions in nucleation experiments, we modeled the laboratory setup[1] with the computational fluid dynamics code FLUENT[19] and the fine particle model (FPM).[20] With this approach, it is possible to determine the nucleation zone, nucleation time, and, therefore, nucleation rates. Also, the model enables us to determine the exact conditions in the nucleation zone and thus compare experimental results and theoretical predictions. The model allows us to establish a nucleation rate profile, which is experimentally impossible to do. By comparing experimental and theoretical results we are able to evaluate the nucleation rate formulations and their predictive powers.

2. Methods

2.1. Description of the Flow Tube. The flow tube is positioned vertically, and its whole length is about 3 m. The experimental setup consists of five main parts: an atomizer, a furnace, a mixing unit, a nucleation chamber, and a particle detection unit; see Figure 1. A liquid sulfuric acid solution of known concentration and amount (0.22 mL/min) is introduced by a HPLC pump (Waters 515) through a ruby micro-orifice together with particle-free sheath air (about 4 L/min) into a furnace, in which the dispersion is vaporized. For each concentration of sulfuric acid, the concentration is analyzed by ion chromatography. This way, the initial concentration of total sulfate injected into the tube is known for every data point. Right

* To whom correspondence should be addressed. E-mail: erik.herrmann@helsinki.fi.
† University of Helsinki.
‡ Finnish Meteorological Institute.
§ Institute of Chemical Process Fundamentals ASCR.
∥ Leibniz-Institut für Troposphärenforschung.
⊥ Particle Dynamics GmbH.

10.1021/jp103499q

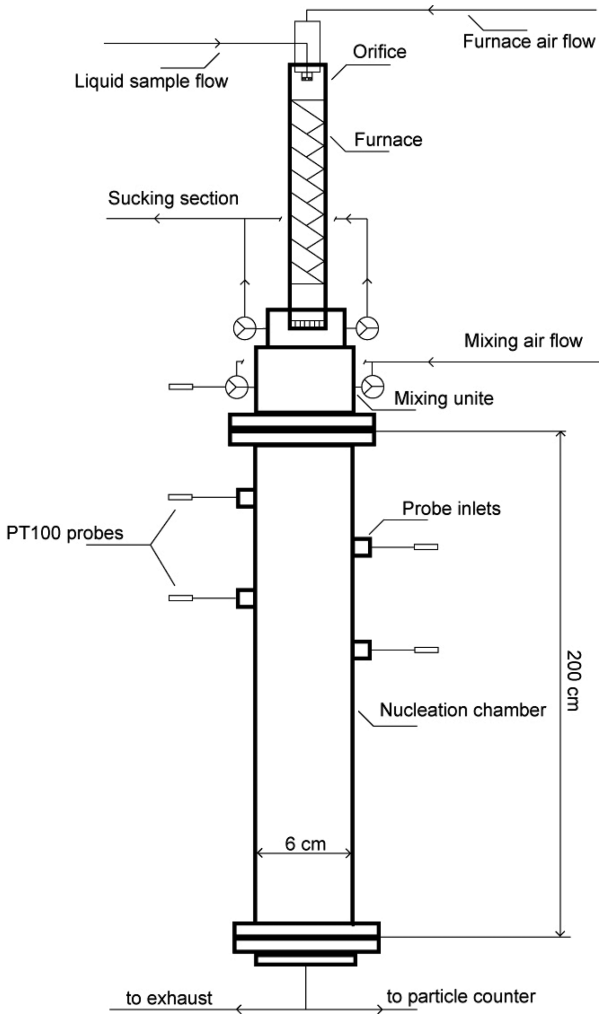

Figure 1. Schematic overview of the experimental setup

after the furnace, the vapor is filtered with a Teflon filter and then introduced into a mixing unit made of Teflon and cooled by turbulent mixing with room-temperature particle-free humid air to about 320 K. The flow rate of the mixing air is about 8 L/min. The vapor−gas mixture is then further cooled in the nucleation chamber, which is kept at a constant temperature (298.15 K) with two liquid circulating baths. Under appropriate conditions, the cooling of the mixture of sulfuric acid and water vapor and air results in the formation of new particles. The nucleation chamber is made of stainless steel; its inner diameter is 6 cm, and the entire length is 200 cm. Concentration of water vapor is measured in the middle and at the end of the nucleation chamber (see figure 1) with two humidity and temperature probes, Vaisala HMP37E, and the humidity data processor, Vaisala HMI38, with 3% accuracy. The aerosol number concentration is measured just after the nucleation chamber with an ultrafine condensation particle counter (UCPC TSI 3025A).

2.2. Modeling. ***2.2.1. FLUENT-FPM.*** To describe fluid flow and particle dynamical processes inside the flow tube, we used the computational fluid dynamics (CFD) code FLUENT[19] in combination with the fine particle model (FPM).[20]

FLUENT models flow based on the Euler equations for mass (eq 1) and momentum (eq 2) conservation.

$$\frac{\partial \rho}{\partial t} + \nabla\cdot(\rho\vec{v}) = S_m \qquad (1)$$

$$\frac{\partial}{\partial t}(\rho\vec{v}) + \nabla\cdot(\rho\vec{v}\vec{v}) = -\nabla p + \nabla\cdot\bar{\tau} + \rho\vec{g} + \vec{F} \qquad (2)$$

Here, S_m is a source term, $\bar{\tau}$ is the stress tensor, $\vec{g}$ is the gravitational and $\vec{F}$ the external body force. ρ, v, p, as usual, stand for density, velocity, and pressure, respectively. In addition, the energy equation (eq 3) is solved.

$$\frac{\partial}{\partial t}(\rho E) + \nabla\cdot(\vec{v}(\rho E + p)) = \nabla\cdot(k_{\text{eff}}\nabla T - \sum_j h_j\vec{J}_j + (\bar{\tau}_{\text{eff}}\cdot\vec{v})) + S_h \qquad (3)$$

In eq 3, k_{eff} is the effective conductivity, and $\vec{J}_j$ is the diffusion flux of species j. The terms on the right represent energy transfer due to conduction, species diffusion, and viscous dissipation, respectively. S_h includes the heat of chemical reaction and other possible volumetric heat sources that have been defined, for example, heat released in the condensational growth of particles.

These equations are solved using a control-volume-based technique that divides the simulation domain into discrete control volumes (grid cells) on which the governing equations are integrated to build equations for the discrete dependent variables (velocity, pressure, etc.). These discretized equations are then solved to obtain updated values of the dependent variables. Because of the nonlinearity of the governing equations, several iterations (depending on the convergence criteria up to several thousands) of the solution loop are necessary to reach convergence. A typical FLUENT simulation calculates the following quantities for each cell of the simulation domain: pressure, density, velocity, temperature, and the mass fraction of the considered species. Additional quantities can be studied by adding user-defined functions (UDF).

The FPM is a complex UDF that provides an aerosol dynamics model for FLUENT. The FPM simulates formation, transformation, transport, and deposition of multicomponent particles in gases and liquids. The FPM describes the dynamics of a particle population, which means that a statistically significant number of particles must exist in the simulation domain, such that their size distribution can be represented by a continuous function. The FPM represents the particle size distribution by a superposition of log-normal size distribution functions (modes). The particle dynamic equations are solved using the moment method; integral moments of the modes (for example total number) become additional scalars in FLUENT.

Using this combination of a fluid and a particle dynamical model (in the following called FLUENT-FPM), the following processes were considered: fluid momentum, vapor mass transfer (including multicomponent diffusion and vapor sink due to condensation to the wall and to particles), heat transfer, nucleation in the water−sulfuric acid system, and particle growth by condensation of sulfuric acid and water vapor. Processes considered also include thermophoresis, latent heat release, and coagulation. Because of small temperature gradients and low nucleation and growth rates, however, these last-mentioned processes have no noticeable effect on the results. During the solution process, continuity, x-velocity, y-velocity, energy, H_2O, H_2SO_4, and four additional scalars that contain the FPM are monitored.

Properties and capabilities of FLUENT and the FPM that are relevant in our simulations as well as most central equations are described in more detail in previous papers on CFD in nucleation studies.[21−23] Fundamental changes to these earlier

works are the inclusion of a binary nucleation parametrization and a new growth law for the particles formed in the process.

2.2.2. Nucleation Rates and Particle Growth. Various nucleation rates are available to describe the formation of new particles in the water−sulfuric acid system. The calculation of a classical binary nucleation rate inside every grid cell of the simulation domain is computationally very expensive. For this reason, we have instead used a nucleation rate parametrization[24] that reduces computing time by a factor of 1/500. This parametrization uses the model for the hydrate formation relying on ab initio calculations of small sulfuric acid clusters and on experimental data for vapor pressures and equilibrium constants for hydrate formation. It is valid for temperatures between 230.15 and 305.15 K, relative humidities from 0.01 to 100%, and sulfuric acid concentration between 10^4 and 10^{11} cm^{-3}. These conditions are met in the experiments[1] underlying our simulations. Moreover, it has to be pointed out that the parametrization is valid only for nucleation rates between 10^{-7} and 10^{10} cm^{-3} s^{-1}. Also, despite its wide nominal relative humidity range, according to the authors, the parametrization works best for RH > 30%.

An alternative path to new particle formation is the collision-controlled or kinetic nucleation mechanism,[25] where the nucleation rate can be described as

$$J = K[H_2SO_4]^2 \tag{4}$$

Here, K is the kinetic coefficient, and $[H_2SO_4]$ is the sulfuric acid vapor concentration. Ambient measurements have yielded values between 10^{-14} and 10^{-11} cm^3 s^{-1} for K.[26−28] In this work, we use a value of 2.5×10^{-14} cm^3 s^{-1}. The activation of pre-existing clusters has been presented as another possibility to form new particles.[29] In this cluster activation theory, the nucleation rate can be written

$$J = A[H_2SO_4] \tag{5}$$

where A is the activation coefficient. For ambient data, values for A between 10^{-7} and 10^{-5} s^{-1} have been found.[26,27] In this work, we use $A = 10^{-6}$ s^{-1}. Both the kinetic nucleation approach and the cluster activation theory are valid for sulfuric acid concentration between 10^5 and 10^{11} cm^{-3}.

To estimate particle growth by condensation of water and sulfuric acid vapors unto the freshly nucleated particles, we implemented a simple growth law:[6]

$$\frac{dD_p}{dt} = \frac{M_s \bar{c} \alpha (C_{vap} - C_{eq})}{2\rho} WR \tag{6}$$

Here, D_p is the particle diameter, ρ its density, M_s is the molecular weight of sulfuric acid, $\bar{c}$ is the mean velocity of H_2SO_4 vapor molecules, and C_{vap} is the concentration of H_2SO_4 vapor. The mass transfer accommodation coefficient α is assumed to be 1, and the equilibrium concentration of H_2SO_4 vapor C_{eq} is assumed to be 0. WR is the ratio of the wet (H_2SO_4 and H_2O) to the dry (only H_2SO_4) diameter. This ratio depends on relative humidity RH and particle diameter D_p, but, neglecting the Kelvin effect, it is only a function of RH and can thus be assumed to be constant at constant relative humidity. Values of WR as a function of RH are given in the literature.[6] Using this growth law implies that growth due to water vapor uptake is not solved dynamically. Instead, particles are assumed to be in equilibrium and water content is determined under this assumption.

2.2.3. Simulation Setup. In the simulations, we only take the nucleation chamber into account. Exploiting the symmetry of the chamber, the problem can be reduced to an axisymmetric simulation. Our 2D grid has a resolution of 50 radial $\times 1000$ axial cells. Since the actual flow profile at the beginning of the nucleation chamber is unknown, the inlet velocity is assumed to be constant over the whole inlet, with the total volume flow matching the experimental setup. The incoming flow's temperature is chosen in such a way that the measured and simulated temperature values match at 20 cm into the tube, which is the first available measurement point. As in the experiment, the wall is set to a temperature of 298.15 K. The wall is assumed to be an infinite sink for sulfuric acid, which means that the H_2SO_4 concentration at the walls is set to 0 in the simulations. Since the wall temperature is well above the water dew point at the chosen conditions, water vapor is assumed to be in equilibrium at the walls, that is, a zero flux boundary was applied. The diffusion coefficient of H_2SO_4 vapor in humid air is set to a constant value of 0.06 cm^2 s^{-1} in all simulations (except where otherwise stated) based on a comparison of experimentally determined sulfuric acid vapor profiles and a series of simulations with the diffusion coefficient as the free parameter. According to experimental results, particles grow only very little (up to about 3 nm, with initial sizes between about 1.5 and 1.9 nm), that is why a unimodal size distribution can be considered sufficient to treat particle formation and growth. Properties of the materials used in the simulations are listed in the appendix.

It has to be pointed out that the model, while being relatively complex and including a large number of processes, nevertheless has to be considered semiquantitative since it still features various important assumptions. These include the validity of the different rate expressions applied to predict the nucleation rate, the profile of the incoming flow, and wall boundary conditions for water and sulfuric acid vapors. However, applying the model to the flow tube in question will provide valuable insights into the details particle formation in this experiment and in general that cannot be gained experimentally.

3. Results

3.1. Flow Characterization. When cooling a downward flow as in the experimental setup, the laminar flow profile can be disturbed by convection. Figure 2 illustrates the effect. In Figure 2A, Reynolds, Grashof, and Archimedes numbers are presented along the center line of the tube. The Grashof number approximately describes the ratio of buoyancy and viscous force, and the Archimedes number compares the relative strength of free and forced convection. Figure 2B shows how the velocity profile across the tube changes as a function of distance from the inlet. Both figures demonstrate that the cooling of the flow results in the formation of an "island" of lower flow velocity around the center of the tube that extends far into the tube but whose influence is strongest during the first half meter of the tube (Reynolds and Archimedes numbers in Figure 2A). With the temperature slope decreasing (Figure 2A), the flow approaches a laminar profile (Figure 2B). Reynolds and Grashof numbers in Figure 2A are both well below transitional values to turbulent flow. This means that although the flow profile itself (Figure 2B) is not that of an ideal laminar flow, the flow is still not turbulent. The Archimedes number profile shows that the first 50 cm are influenced by buoyancy driven convection ($Ar \gg 1$), whereas after 50 cm in the nucleation chamber, forced convection ($Ar \ll 1$) starts to dominate.

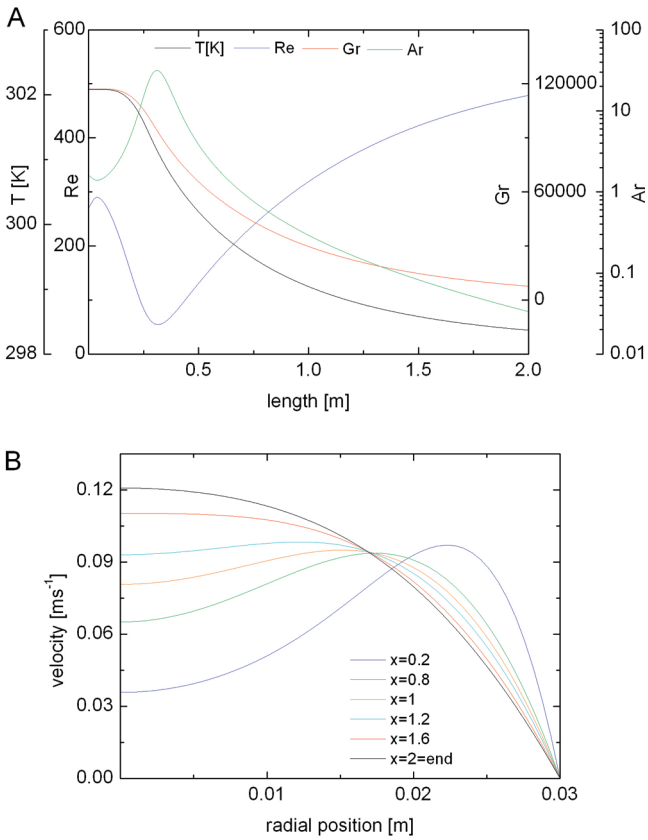

Figure 2. Details of the flow inside the nucleation chamber. A: The typical profiles of Reynolds (Re), Grashof (Gr), and Archimedes (Ar) numbers as well as temperature (T) on the center line of the tube as a function of the nucleation chamber distance. The first 50 cm are influenced by buoyancy driven convection (Ar $\gg$ 1), after 50 cm in the nucleation chamber starts to dominate forced convection (Ar $\ll$ 1). B: Velocity profiles across the tube at various distances from the inlet.

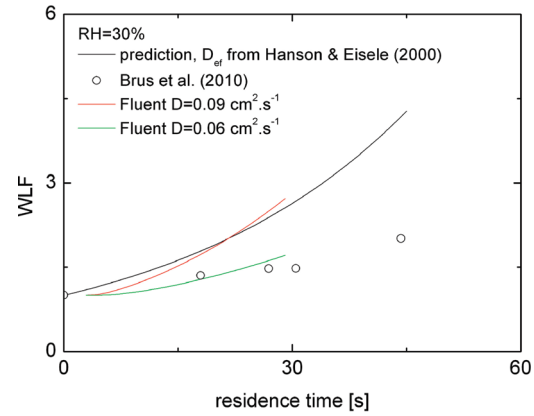

Figure 3. Wall loss factors (WLF) of sulfuric acid RH = 30% in the experiment, simulated for two diffusion coefficients, and estimated with the diffusion coefficient of sulfuric acid in humidified nitrogen.[31]

The simulated nucleation maximum typically lies around 70 cm, which means that the peak occurs only after the main impact zone of convection. Since convection slows down the flow in the center of the tube, it follows that the nucleation peak is moved closer to the tube inlet. After the nucleation peak, particles reside on the center line of the tube for about 14s before reaching the outlet. If the flow was laminar, from 70 cm to the outlet would pass only about 10 s. If one also takes into account that a (hypothetical) well developed parabolic velocity profile[30] would shift the nucleation peak further downstream, one must conclude that convection effects significantly increase the residence time of center line particles and thus their possibilities to grow to detectable sizes.

3.2. Temperature, Vapor Profiles, and Wall Losses. In the flow tube, sulfuric acid vapor is constantly lost to the walls. This affects the H_2SO_4 concentration profile and thus the nucleation rate and particle growth. Figure 3 shows a comparison of the experimentally determined wall loss factor (WLF) to theoretical prediction of WLF using the RH dependent diffusion coefficient of sulfuric acid in nitrogen[31] and FLUENT-FPM simulations with two different diffusion coefficients D = 0.09 and 0.06 cm^2 s^{-1}. For RH values of 10, 30, and 50% simulation results and experimental data show good agreement when the diffusion coefficient is chosen to be 0.06 cm^2 s^{-1}. Theory predicts an influence of RH on the diffusion coefficient, and although a close comparison of simulations with a constant diffusion coefficient to measurements at 10, 30, and 50% RH reveals slight differences, the experimental data does not allow quantifying the effect. It has to be noted that the temperature dependence of the diffusion coefficient was not taken into account in the simulations. However, this dependence should have only a rather small effect since the diffusion coefficient is proportional to $\sim T^{1.75}$, and the temperature difference between the incoming flow and tube wall is only a few Kelvin.

Figure 4 shows profiles of temperature and the molar concentrations of water and sulfuric acid vapor for an example setup with RH = 30% and [H_2SO_4] = 4 $\times$ 10^9 cm^{-3}. Figure 4A illustrates how the flow is cooled by the walls. Since water vapor is assumed not to condensate on the walls, Figure 4B is very closely related to 4A. In fact, 4B can be considered the "negative" of 4A, since only the decrease in temperature leads to the rise in molar concentration, that is, density. One has to note, that despite the wide color range, the change in absolute numbers is very small, with the complete scale spanning only 1.5%. Figure 4C finally shows the molar concentration of sulfuric acid vapor and how the vapor is lost to the walls.

Naturally, sulfuric acid is also consumed by the formation and growth of new particles. As will be discussed later, these losses are well below 1 promille of the incoming vapor over the whole length of the nucleation tube even for the highest nucleation rates considered in this study and thus much smaller than the experimental uncertainty in determining the concentration of sulfuric acid vapor.[1] To the walls, about 50% of all sulfuric acid are lost. Similarly, water vapor losses to newly formed particles have an even smaller effect on the profile depicted in Figure 4B: the water content of the particles is of the same order of magnitude as their sulfuric acid content, but water is much more abundant. Thus, to affect the sulfuric acid or even the water vapor profiles, one would have to implement nucleation rates that are several orders of magnitude larger than the ones observed in the experiment.

3.3. Nucleation Zone. To study the characteristics of the nucleation zone, the nucleation rate gained from the binary nucleation parametrization was used. This rate is widely used and, among the rates discussed here, it is the only one to take into account temperature and relative humidity. Figure 5 shows the nucleation rates normalized with respect to peak height for RH values of 10, 30, and 50%. Flow and H_2SO_4 vapor concentration values have been set to be identical in all three simulations. The figure shows that the location of the maximum theoretical nucleation rate J_{theo} (binary) is not significantly depending on relative humidity. However, with growing relative humidity, the nucleation zone grows, that is, the nucleation peak in Figure 5 becomes wider. This is an expected result: with

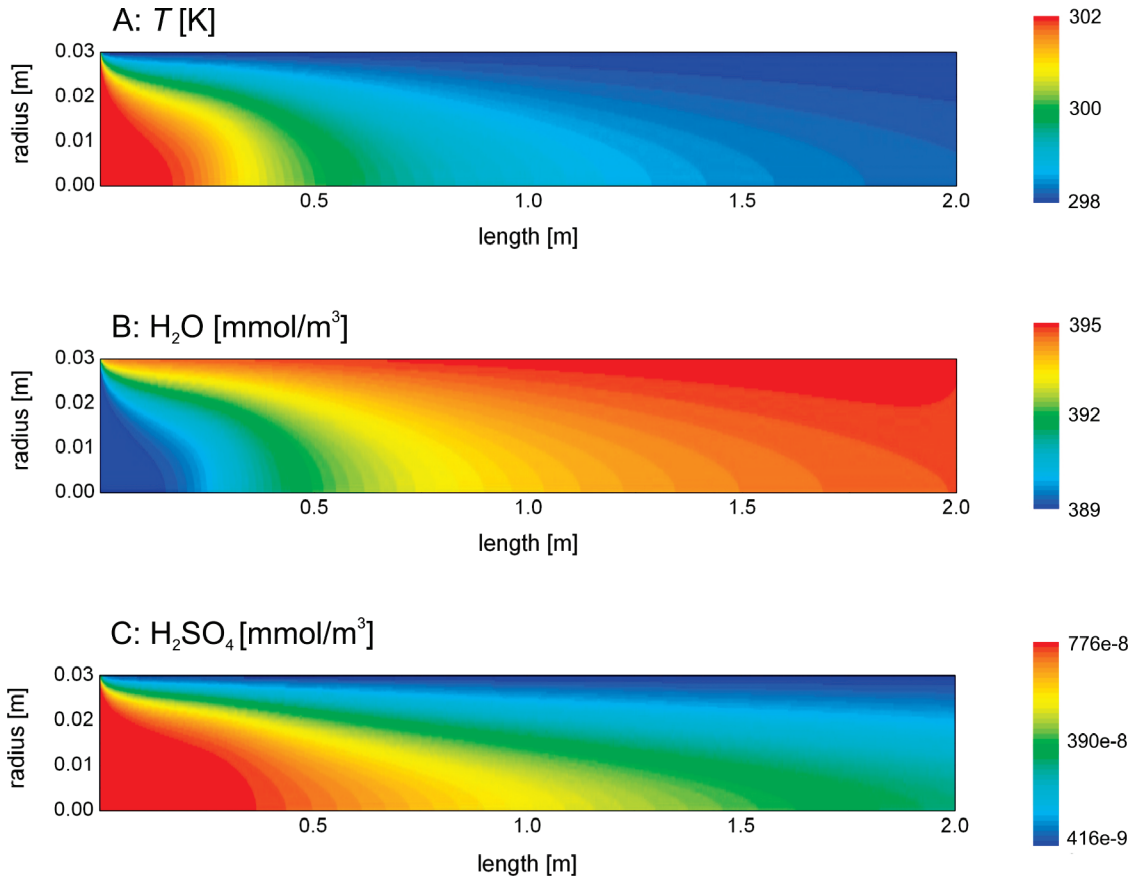

Figure 4. Profiles of temperature (A) and molar concentration of water (B) and sulfuric acid (C) vapors.

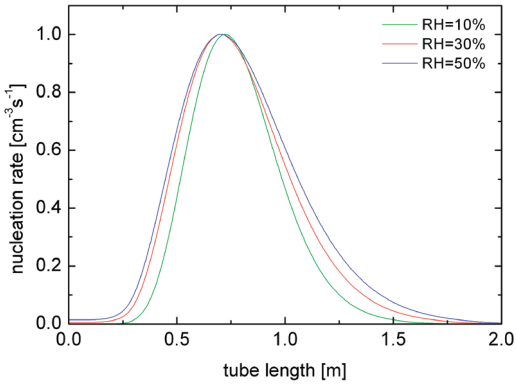

Figure 5. Nucleation rate on the center line of the tube as a function of position on the center line for three values of relative humidity. Normalized values.

otherwise identical parameters, higher relative humidity of course leads to more nucleation. In detail, this means that higher RH widens the nucleation zone toward the tube inlet by counteracting the high initial temperature that prohibits nucleation. Downstream of the maximum, higher RH widens the nucleation zone by compensating for the losses of H_2SO_4 vapor, which at lower RH would have already meant the end of nucleation.

Depending on the flow rate and sulfuric acid vapor concentrations, the nucleation maximum in our simulations has been found to be located between 54 and 65 cm (RH = 10%) and 65 and 76 cm (RH = 30% and 50%) into the nucleation tube. With growing H_2SO_4 vapor concentrations, the nucleation rate maximum moves closer to the tube inlet. This explains the different nucleation zone positions for different relative humidity values: for RH = 10%, experimental and thus also simulated H_2SO_4 vapor concentration values were higher than for 30 and 50% RH.

Figure 6 shows the binary nucleation rate and the particle number concentration profiles for residence times 30 and 45 s. The nucleation rate profile for 30s residence time (the standard setup in experiment and simulation) depicts the main nucleation area at the center of the tube between 0.5 and 1.0 m (Figure 6A). We can also see that nucleation, if only at a very small rate, starts earlier in the tube, almost at the inlet, close to the wall. The wall cools the incoming gas−vapor mixture, thus making nucleation possible. The picture indicates that, in our setup, temperature is the decisive parameter that controls the onset of nucleation. CFD simulations of another system have similarly shown that the activation of silver particles in a TSI 3785 water−CPC first starts off the center line of the instrument.[23] For 45 s residence time, the nucleation rate profile looks very similar, only shifted closer to the tube inlet (main nucleation area between 0.3 and 0.6 m) and skewed in flow direction (Figure 6C). Also, the nucleation area appears to be slightly wider in radial direction.

The particle number concentration for 30 s residence time (Figure 6B) shows how nucleation rate and particle number concentration relate to one another. The number concentration reaches its peak (between 1.0 and 1.25 m) after nucleation (Figure 6A) has ceased for the most part. Similar observations can be made when comparing nucleation rate and particle number concentration profiles for a residence time of 45s (Figures 6C and 6D). Particle number concentration profiles (Figures 6B and 6D) suggest that most particles remain in the wake of the nucleation zone for their remaining time in the tube. The profiles also show how particle concentration profiles evolve

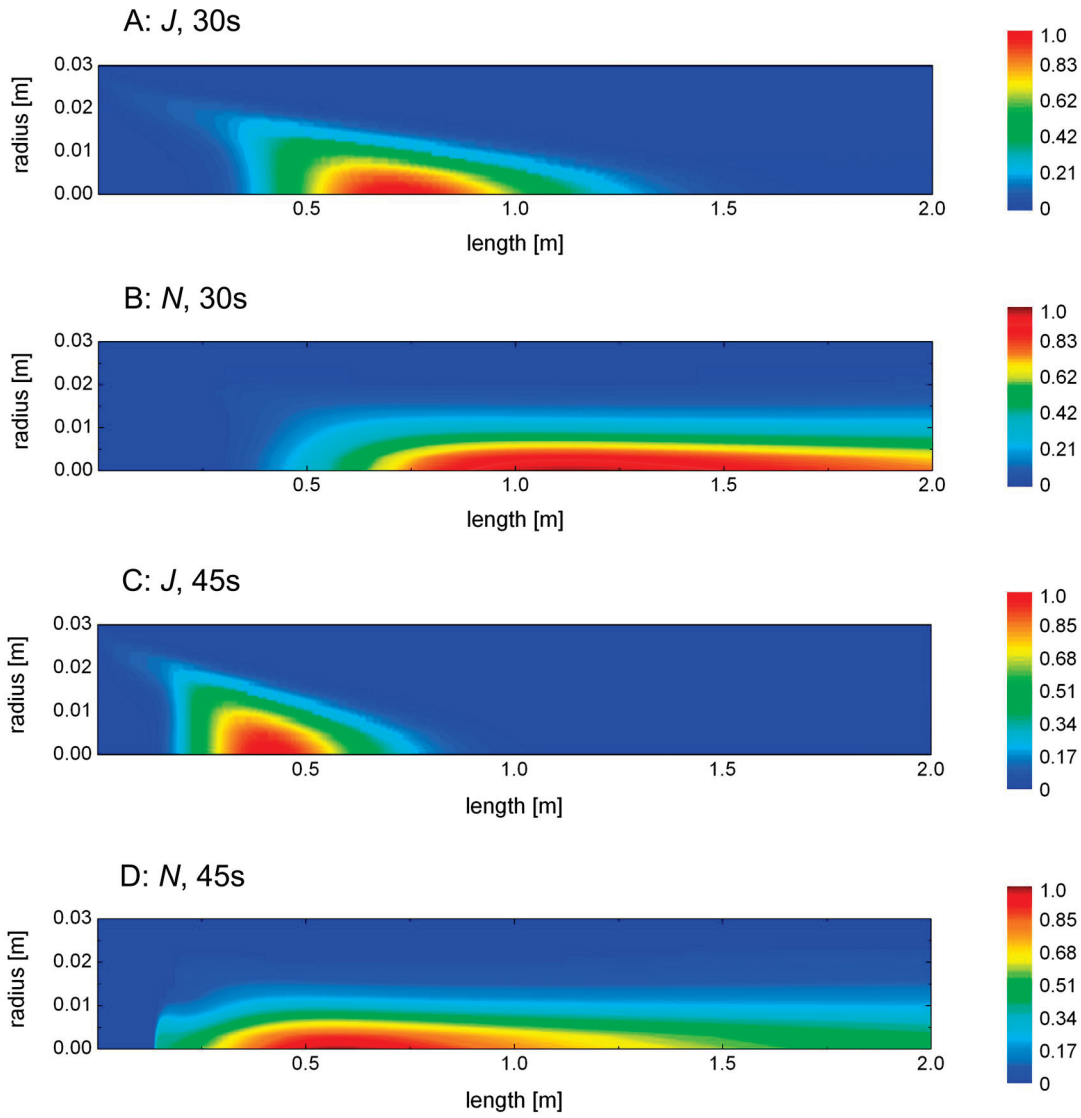

Figure 6. Binary nucleation rate and particle number concentration profiles for residence times 30 and 45 s. Otherwise identical setup. Normalized values.

over time, controlled by diffusion and the particle sink at the wall. Naturally, this can best be seen for 45 s residence time (Figure 6D).

Although nucleation rate profiles cannot be measured directly, particle number concentration profiles can. However, a detailed comparison of experiment and simulation is problematic. Whereas the simulation result (Figures 6B and 6D) includes all particles present in the tube, the measurement can include only those that can be detected. In the experiment,[1] the pulse-height CPC was used, which is able to detect particles with a mean mobility diameter of 1.5 nm. This means that, depending on their initial diameter, particles possibly have to grow before being detectable, and even then the instrument's counting efficiency is much smaller than 1. This results in a distorted and shifted picture when comparing experiment and simulation. The measured nucleation zones for residence times 30 and 45 s start at about 60 and 90 cm from the beginning of the nucleation chamber, respectively.[1] The simulations (Figures 6B and 6D) show significant particle concentrations already at 50 and 20 cm for 30 and 45 s residence time, respectively. This suggests that particles in the experiment are not detected where they are formed but only after growing to detectable sizes, that is, downstream from their area of formation.

3.4. Nucleation Rates in Simulation and Experiment. Figure 7 shows nucleation rates (left column) and number concentrations (right column) as a function of sulfuric acid vapor concentration for relative humidities of 10, 30, and 50% (A, B, and C, respectively). The left column compares various nucleation rates. In the figure, "FMI experiment" denotes the experimental nucleation rate derived from the measured particle number concentration N by dividing it by half the residence time.[1] From these slopes has been estimated that the critical cluster contains 8, 6, or 4 sulfuric acid molecules for relative humidities 50, 30, and 10%, respectively.[1] "Binary nucleation", "Kinetic nucleation", and "Cluster activation" denote the nucleation rates derived from the respective theories. The experimental nucleation rate in Figure 7 is merely a scaled view of the experimentally determined particle concentration. A comparison of the left and right column underlines this. Comparing experimental results and binary nucleation rates, one finds that for 10 and 30% RH binary nucleation theory predicts much steeper slopes than found in the experiment. As a result, absolute nucleation rate values differ very much for low sulfuric acid concentrations while they approach one another for higher acid concentrations. One has to point out that the binary nucleation parametrization used to gain these nucleation rates

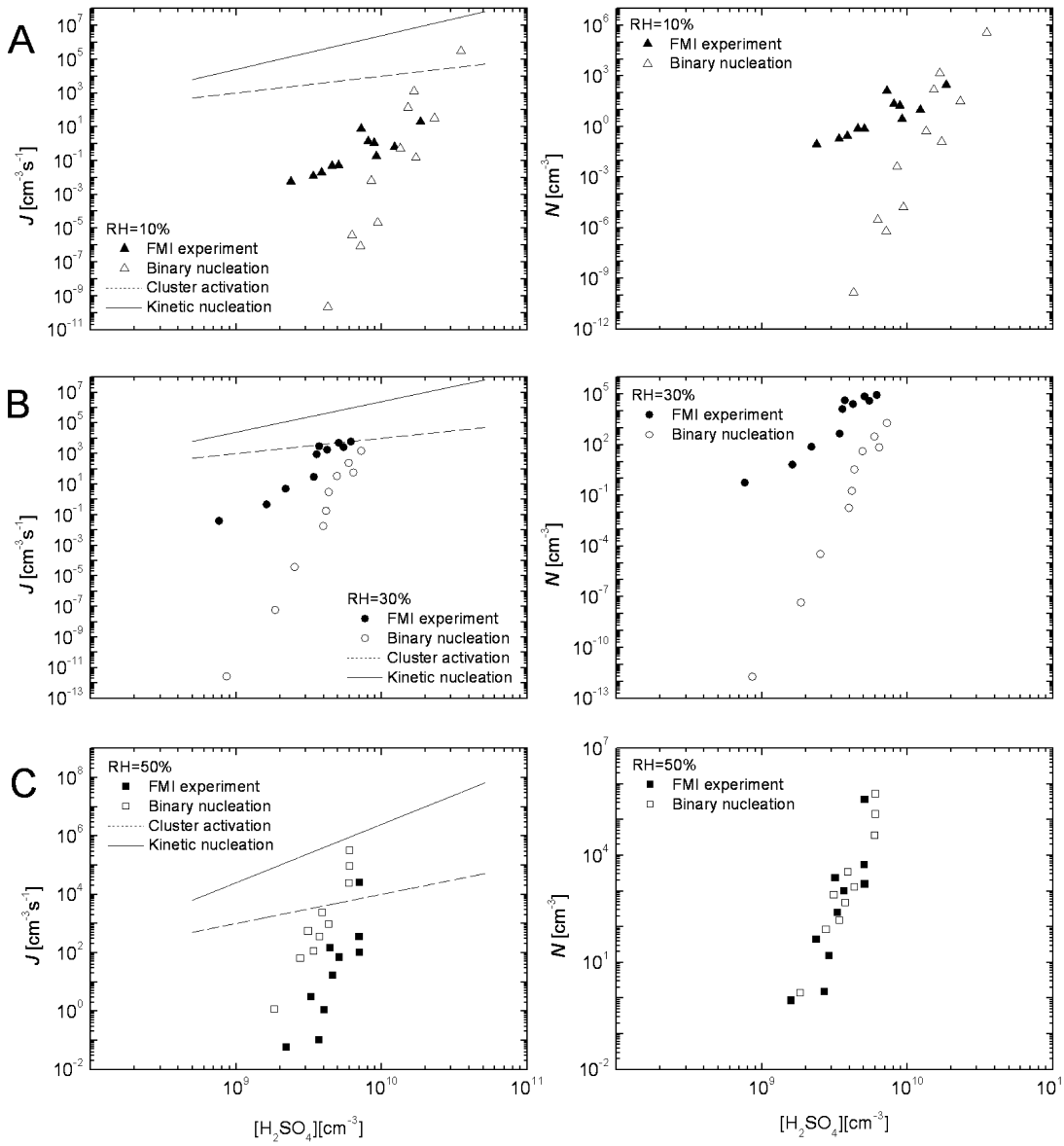

Figure 7. Number concentration N and nucleation rate J as a function of sulfuric acid concentration for RH values of 10, 30, and 50%. Comparison of experimental results to various theoretical nucleation rates and simulated number concentration.

is not valid for nucleation rates below 10^{-7} cm^{-3} s^{-1}, which concerns the lower end of the binary nucleation rate at 10 and 30% RH. At RH = 50%, the slope of the binary nucleation rate and the experimental nucleation rate are approximately the same. This is in good agreement with the authors' assessment[24] of the validity of their parametrization that it works best for relative humidities over 30%.

Ignoring the absolute values, which are largely uncertain as the range for A and K shows, the slope of both kinetic nucleation and cluster activation is shallower than the experimental one. This highlights the limitations of the experimental setup. For low sulfuric acid concentrations, particle growth is so limited that the CPC with its cutoff diameter of 2.18 nm will simply not detect a large portion of the particles, resulting in a significant undercount under these conditions. However, at 10 and 30% RH, the difference between the experimental slope and kinetic nucleation is not very dramatic, indicating that the kinetic theory might describe nucleation quite realistically for these relative humidities. At 50% RH, the situation is different; the difference between the experimental and the kinetic slope is much larger. Because we do not expect an even more significant undercount here, the cause lies probably with the kinetic nucleation approach that ignores the role of water in the nucleation process. Upon closer inspection, we also see that indeed at 10% RH, the slopes of experiment and kinetic nucleation are closer to one another than at 30%, which supports this conclusion. Summarizing, the left column illustrates how kinetic nucleation works better at low relative humidities whereas the binary nucleation parametrization yields better results at higher RH values.

In the case of particle number concentration N (right column), a direct comparison of experimental data and simulation results is presented. On the basis of the binary nucleation rate, FLUENT-FPM has simulated how many particles would be counted at the tube outlet. Here, this number ("binary nucleation") is compared to its experimental counterpart ("FMI experiment"). Because the experimental nucleation rate (left column) is merely a scaled version of the number concentration, the experimental curves in the left and in the right column are basically the same. More interestingly, also the simulated number concentration behaves very much like the binary nucleation rate in the left column. This indicates that the ratio

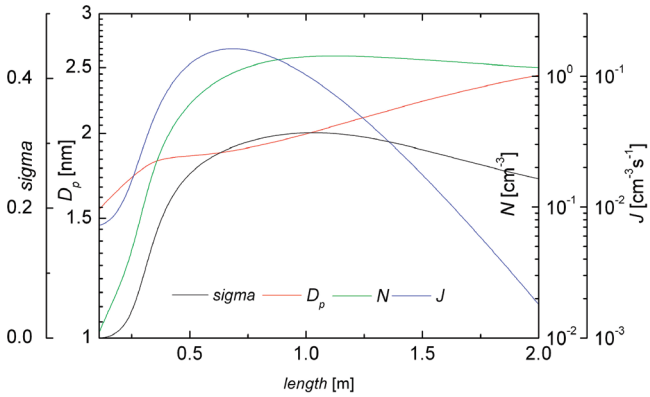

Figure 8. Binary nucleation rate J, particle number concentration N, mean particle diameter D_p, and standard deviation σ on the center line of the tube.

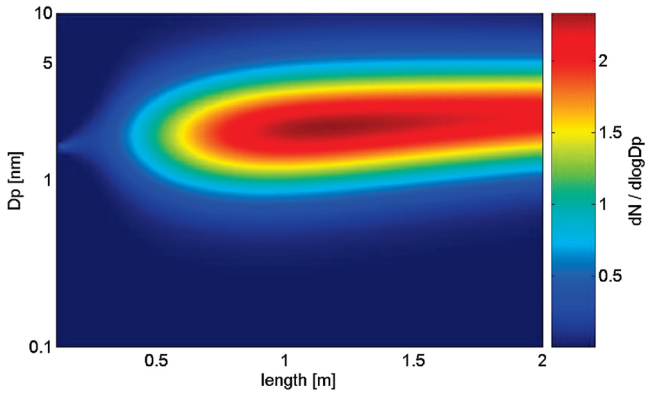

Figure 9. Evolution of the particle size distribution on the center line of the tube as predicted by FLUENT-FPM. The setup is the same as in Figure 7.

between theoretical nucleation rate and modeled number concentration is approximately a constant, which describes the experimental and simulation setup. Hence, it is possible to scale the binary nucleation rate based on the results in the right column in order to improve its performance.

3.5. Growth. Figures 8 and 9 show nucleation and growth of particles on the center line of the tube for an example case with RH = 50% and a sulfuric acid vapor concentration of 9.84×10^9cm^{-3}. The initial particle size (i.e., the critical cluster size) and the nucleation rate is predicted by the same parametrization as above.[24] The first particles nucleate and grow before the beginning of the actual nucleation peak (ca. 0.1−0.3 m) (Figure 8). With the beginning of the main nucleation zone, growth seems to slow down or even stop for a while. However, the diameter depicted in Figure 8 is the mean diameter of the whole particle population. The figure shows that in addition to the older particles, which have already grown to some extent, new smaller particles are formed. The growth of the mean diameter of the whole population thus appears to stagnate. Simultaneously, while most new particles are formed, the width of the particle size distribution, described by the standard deviation σ, grows rapidly. The particle growth rate picks up again shortly before the nucleation rate maximum is reached, that is, when the production of new particles does not dominate the total number concentration anymore. In line with this, the width of the particle distribution (Figure 9) slightly decreases after the nucleation peak has been passed. After about 1 m, the particle number concentration on the center line decreases (Figure 8). At this point, new particle formation no longer produces enough new particles to replace particles that have diffused away from the center line. At the tube outlet, particles on the center line have a mean diameter of 2.44 nm according to this simulation. Averaged over the entire outlet, the mean diameter is 2.34 nm. Under the same conditions, the measured mean diameter was found to be 2.2 nm.[1]

With its high sulfuric acid concentration, 50% RH, and the resulting relatively high nucleation rate, the case depicted in Figures 8 and 9 can be used to estimate an upper limit for the sulfuric acid vapor losses due to formation and growth of particles. At a measured particle number concentration of 70 000 cm^{-3} and with a sulfuric acid content of the particles of about one-third,[6] the total sulfuric acid content of the particles at the tube outlet is about 0.5 promille of the total H_2SO_4 losses.

Generally, particle number concentrations and growth rates are so small that vapor depletion does not noticeably affect the results.

3.6. Discussion of Main Model Assumptions and Their Implications. The model as a whole contains various assumptions that can affect the simulations' outcome. The most central assumptions concern the flow profile at the flow inlet, the wall boundary conditions, and the diffusion coefficient of sulfuric acid vapor in humid air. The material properties (except for said diffusion coefficient) and their uncertainties most likely do not influence the results significantly. Air can be assumed to be rather well-known, the same applies for water vapor, and the sulfuric acid vapor concentration is so low that the properties of sulfuric acid vapor will not affect the characteristics of the flow. As pointed out earlier, feedback of nucleation and growth on vapor and temperature profiles is minimal.

Assuming, for the sake of the argument, laminar flow throughout the tube, it is clear that the choice of inlet boundary condition affects the results. Using a parabolic inlet velocity profile instead of the constant velocity assumption used here, various profiles would be shifted somewhat toward the tube inlet, the shift being of the order of magnitude of the entry length for our tube. This would affect the results quantitatively, but the effect would concern all profiles, and thus qualitatively one would expect the same results. However, this is speculative: the flow profile is *not* parabolic throughout the tube. The cooling of the flow causes convection, and this convection significantly reduces the effect of the chosen velocity profile at the tube inlet. Convection "levels the ground". Additionally it has to be pointed out that the geometry of the experimental setup (see Figure 1) does not suggest a parabolic flow profile as the most probable scenario: the mixing unit is too short to establish laminar flow after turbulent mixing.

In the simulations, the sulfuric acid concentration at the wall is set to 0. Alternatives to this assumption are no diffusion to the wall at all and a wall concentration greater than 0. No sulfuric acid diffusion to the wall is an option in stark contrast to experimental findings: almost 50% of sulfuric acid is lost in the tube, and judging by the size and number of particles, it is clearly not lost to the particles. A wall concentration other than 0, however, has not been disproved experimentally. The problem is the following: from the point of view of center line acid concentrations, wall concentrations larger than 0 and a smaller diffusion coefficient have the same effect. To disentangle boundary conditions and diffusion coefficient requires exact measurements of the sulfuric acid profile, with special focus on the profile in radial direction. Such data is not currently available. In our simulations, we have used 0.06 cm^2 s^{-1} as the diffusion coefficient of sulfuric acid in humid air. Together with the assumption of zero acid concentration at the wall, this yields good agreement with experimental data (see Figure 3). Test

TABLE A1: Parameters to Calculate the Heat Capacity of Water and Sulfuric Acid Vapor

	A	*B*	*C*	*D*	*E*
water	1885.167	−0.4677	0.001661	-9.903×10^{-7}	2.052×10^{-10}
sulfuric acid	96.717	3.446	−0.003882	2.173×10^{-6}	-4.78×10^{-10}

simulations have shown that alternative scenarios with nonezero sulfuric acid concentration at the wall and a different diffusion coefficient would result in shifted nucleation rate profiles (compare Figures 6A and 6C). Additionally, the nucleation rate profile would be wider in radial direction. However, the general qualitative findings of our simulations are quite robust with respect to such alterations.

With sulfuric acid at the wall, one has to consider the possibility of water condensing on the wall, even though the wall temperature is well above the dew point. However, measurements of relative humidity have not shown significant water losses inside the tube. This means that even if there are losses, they are not very large, and the assumption of no vapor losses to the wall is well within experimental accuracy. This, again, shows that the improvement of the model requires first and foremost more exact measurements of the experimental conditions.

4. Conclusions

In this work, we have simulated a series of experiments on the formation of new particles in the water-sulfuric acid-system with the CFD code FLUENT and the aerosol dynamics model FPM. The formation of new particles was described with a parametrization of classical nucleation theory as well as with a kinetic nucleation rate and the cluster activation theory.

Concerning the flow characteristics in the tube, we found that convection plays a significant role during the first 0.5 m of the tube. In this part of the simulation domain, we observed an area of low flow velocity around the tube's center line. Ultimately, convection effects prolong the residence time in the tube for particles on and close to the center line. Compared to a hypothetical laminar flow profile, those particles have more time to grow.

Nucleation behavior was simulated for RH values of 10, 30, and 50%, with sulfuric acid concentration ranging from 10^9 to 3×10^{10} cm^{-3}. In comparison, atmospheric nucleation has been observed for sulfuric acid concentrations between 10^5 and 10^7 cm^{-3}.[26] CFD simulations allow us to establish a nucleation rate profile. We found the nucleation maximum to be located on the center line between 0.54 and 0.76 m inside the tube. The exact location of the maximum is determined mainly by the total flow rate and the sulfuric acid vapor concentration, while relative humidity plays only a very minor role. With higher residence times, that is, lower flow rates, nucleation moves closer to the tube inlet. In terms of absolute numbers, the binary nucleation rate yielded good agreement with experimental results especially for 50% RH. For 10 and 30% RH, agreement becomes worse for smaller H_2SO_4 vapor concentrations. At these relative humidities, the kinetic nucleation theory predicts nucleation rate slopes that are very close to experimental findings. The growth of newly formed particles was simulated with a relatively simple growth model. For an example case at 50% RH, particles grew to about 2.34 nm mean diameter, which is close to the experimental value (2.2 nm).

The results of this study point out possible improvements to the model. To better determine the inlet flow profile for example, a detailed analysis of the mixing unit and the incoming flows is necessary. Additionally, the diffusion coefficient of sulfuric acid vapor in air as a function of relative humidity and temperature needs to be determined more accurately to replace the current constant approximation. To do this, more measurements are needed. The current model assumes an infinite H_2SO_4 vapor sink at the walls. This assumption needs to be tested experimentally. If the sulfuric acid vapor sink is not infinite, that is, the concentration of H_2SO_4 vapor at the wall cannot be assumed to be 0; an assumption of infinite sink will result in the same errors as too large values for the diffusion coefficient. With these improvements, the model would be more quantitatively reliable.

Our comparison of experimental data and Fluent-FPM simulations of a CNT parametrization to the kinetic nucleation theory and the cluster activation theory show how the different theories work better under different relative humidity conditions. The challenge now is to combine these approaches into one theory. Fluent-FPM then offers a good tool to test this new theory against experimental results.

Appendix

Mixture Properties. The gas mixture in our simulations consists of air, water vapor, and sulphuric acid vapor. The density of the mixture is determined using the ideal gas theory. The mass diffusion coefficient of sulphuric acid vapor in humid air is set to 0.06 cm^2 s^{-1}. Motivations for and consequences of this are discussed in Sections 3.2 and 3.6.

Air. The heat capacity of air is 1.006 kJ/(kg K). In this case a constant value is sufficient since, at given accuracy, the value does not change within the temperature range of the simulations. The thermal conductivity is

$$k = 0.0022 + 8 \times 10^{-5} T \tag{A1}$$

where k is in W/(m K) and T in K. The viscosity is determined by

$$\mu = 4 \times 10^{-6} + 5 \times 10^{-8} T \tag{A2}$$

where μ is in kg/(m s), and T is in K. The Lennard-Jones parameters 3.711 Å and 78.6 K are used to calculate the thermal diffusion coefficient with Fluent's built-in kinetic theory module.

The properties of air as presented here are taken from Granryd's collection of formulas and tables.[32] The Lennard-Jones parameters are readily available in Fluent.

Water Vapor. The heat capacity of water vapor is calculated from a polynomial

$$C_p = A + BT + CT^2 + DT^3 + ET^4 \tag{A3}$$

where C_p is in J/(kg K) and T is in K. The parameters *A, B, C, D,* and *E* are listed in Table A1.

The thermal conductivity of water vapor is determined by

$$k = 0.00053 + 4.7093 \times 10^{-5}T + 4.9551 \times 10^{-8}T^2 \quad \text{(A4)}$$

where k is in W/(m K) and T in K. The viscosity of water vapor is determined by

$$\mu = (-36.826 + 0.429T - 1.62 \times 10^{-5}T^2)10^{-7} \quad \text{(A5)}$$

where μ is in kg/(m s), and T is in K. The Lennard-Jones parameters 2.605 Å and 572.4 K are used to calculate the thermal diffusion coefficient.

The properties of water vapor as presented here are taken from Yaws' standard book.[33] The Lennard-Jones parameters are readily available in Fluent.

Sulfuric Acid Vapor. The heat capacity of sulfuric acid vapor is calculated using eq A3 and the parameters listed in Table A1. The remaining properties of the vapor are scarcely available, especially for the needed temperature range. That is why we have decided to calculate thermal conductivity and viscosity with Fluent's in-built kinetic theory model. The necessary Lennard-Jones parameters were estimated to be 4.677 Å and 716 K with the help of two equations.[34] With those the length parameter is

$$\sigma \simeq 8.33V_c^{1/3} \quad \text{(A6)}$$

and the energy parameter is simply $0.75T_c$. V_c and T_c are critical volume and temperature, respectively, and are presented by Yaws.[33] As for the other material, also in this case the Lennard-Jones parameters are used to determine the thermal diffusion coefficient.

Acknowledgment. This research was supported by the Academy of Finland Center of Excellence program (project No. 1118615). All simulations were performed on the servers of the CSC - IT Center for Science, where Dr. Thomas Zwinger provided valuable technical assistance.

References and Notes

(1) Brus, D.; Hyvärinen, A.-P.; Viisanen, Y.; Kulmala, M.; Lihavainen, H. *Atmos. Chem. Phys.* **2010**, *10*, 2631–2641.
(2) Twomey, A. *Atmos. Environ.* **1974**, *8*, 1251–1256.
(3) Twomey, S. *Atmos. Environ.* **1991**, *25A*, 2435–2442.
(4) Johnson, B. T.; Shine, K. P.; Forster, P. M. *Q. J. R. Meteorol. Soc.* **2004**, *130*, 1407–1422.
(5) Kulmala, M.; Vehkamäki, H.; Petäjä, T.; Dal Maso, M.; Lauri, A.; Kerminen, V.-M.; Birmili, W.; McMurry, P. H. *J. Aerosol Sci.* **2004**, *35*, 143–176.
(6) Seinfeld, J. H.; Pandis, S. N. *Atmospheric Chemistry and Physics: From Air Pollution to Climate Change*; Wiley: New York, 1997.
(7) Clarke, A. D.; Varner, J. L.; Eisele, F.; Mauldin, R. L.; Tanner, D.; Litchy, M. *J. Geophys. Res.* **1998**, *103* (D13), 16397–16409.
(8) Korhonen, P.; Kulmala, M.; Laaksonen, A.; Viisanen, Y.; McGraw, R.; Seinfeld, J. H. *J. Geophys. Res., Atmos.* **1999**, *104*, 26349–26353.
(9) O'Dowd, C. D.; Aalto, P.; Hämeri, K.; Kulmala, M.; Hoffmann, T. *Nature* **2002**, *416*, 497–498.
(10) Bonn, B.; Moortgat, G. K. *Geophys. Res. Lett.* **2003**, *30*, 1585.
(11) Sipilä, M.; Berndt, T.; Petäjä, T.; Brus, D.; Vanhanen, J.; Stratmann, F.; Patokoski, J.; Mauldin, R. L.; Hyvärinen, A.-P.; Lihavainen, H.; Kulmala, M. *Science* **2010**, *327*, 1243–1246.
(12) Crutzen, P. J. *Climatic Change* **2006**, *77*, 211–219.
(13) Wingenter, O. W.; Elliot, S. M.; Blake, D. R. *Atmos. Environ.* **2007**, *41*, 7373–7375.
(14) Reiss, H.; Margolese, D. I.; Schelling, F. J. *J. Colloid Interface Sci.* **1976**, *56*, 511–526.
(15) Viisanen, Y.; Kulmala, M.; Laaksonen, A. *J. Chem. Phys.* **1997**, *107*, 920–926.
(16) Ball, S. M.; Hanson, D. R.; Eisele, F. L.; McMurry, P. H. *J. Geophys. Res.* **1999**, *104* (D19), 23709–23718.
(17) Berndt, T.; Böge, O.; Stratmann, F. *Geophys. Res. Lett.* **2006**, *33*, L15817.
(18) Young, L. H.; Benson, D. R.; Kameel, F. R.; Pierce, J. R.; Junninen, H.; Kulmala, M.; Lee, S.-H. *Atmos. Chem. Phys.* **2008**, *8*, 4997–5016.
(19) Fluent: *FLUENT 6.2 User's Guide*; Fluent Inc.: Lebanon NY, USA, 2005.
(20) Particle Dynamics: *Fine Particle Model (FPM) for FLUENT*; Particle Dynamics GmbH: Leipzig, Germany, 2005.
(21) Herrmann, E.; Lihavainen, H.; Hyvärinen, A.-P.; Riipinen, I.; Wilck, M.; Stratmann, F.; Kulmala, M. *J. Phys. Chem. A* **2006**, *110*, 12448–12455.
(22) Herrmann, E.; Hyvärinen, A.-P.; Brus, D.; Lihavainen, H.; Kulmala, M. *J. Phys. Chem. A* **2009**, *113*, 1434–1439.
(23) Stratmann, F.; Herrmann, E.; Petäjä, T.; Kulmala, M. *Atmos. Meas. Tech.* **2010**, *3*, 273–281.
(24) Vehkamäki, H.; Kulmala, M.; Napari, I.; Lehtinen, K. E. J.; Timmreck, C.; Noppel, M.; Laaksonen, A. *J. Geophys. Res.* **2002**, *107* (D22), 4622.
(25) McMurry, P. H. *J. Colloid Interface Sci.* **1980**, *78*, 513–527.
(26) Sihto, S.-L.; Kulmala, M.; Kerminen, V.-M.; Dal Maso, M.; Petäjä, T.; Riipinen, I.; Korhonen, H.; Arnold, F.; Janson, R.; Boy, M.; Laaksonen, A.; Lehtinen, K. E. J. *Atmos. Chem. Phys.* **2006**, *6*, 4079–4091.
(27) Riipinen, I.; Sihto, S.-L.; Kulmala, M.; Arnold, F.; Dal Maso, M.; Birmili, W.; Saarnio, K.; Teinilä, K.; Kerminen, V.-M.; Laaksonen, A.; Lehtinen, K. E. J. *Atmos. Chem. Phys.* **2007**, *7*, 1899–1914.
(28) Kuang, C.; McMurry, P. H.; McCormick, A. V.; Eisele, F. L. *J. Geophys. Res.* **2008**, *113* (D10), D10209.
(29) Kulmala, M.; Lehtinen, K. E. J.; Laaksonen, A. *Atmos. Chem. Phys.* **2006**, *6*, 787–793.
(30) Bird, R. B.; Stewart, W. E.; Lightfoot, E. N. *Transport Phenomena*; John Wiley & Sons: New York, 1960.
(31) Hanson, D. R.; Eisele, F. L. *J. Phys. Chem. A* **2000**, *104*, 1715–1719.
(32) Granryd, E. *Heat Transfer, Collection of Formulas and Tables of Thermal Properties*; Department of Applied Thermodynamics and Refrigeration, The Royal Institute of Technology KTH: Stockholm, Sweden, 1995.
(33) Yaws, C. L. *Chemical Properties Handbook*; McGraw-Hill: New York, 1999.
(34) Mills, A. F. *Mass Transfer*; Prentice-Hall: Upper Saddle River, NJ, 2001.

JP103499Q